ACS Catalysis

Research Article

pubs.acs.org/acscatalysis

Solar Light Driven Pure Water Splitting on Quantum Sized $BiVO_4$ without any Cocatalyst

Songmei Sun, Wenzhong Wang,* Dezhi Li, Ling Zhang, and Dong Jiang

State Key Laboratory of High Performance Ceramics and Superfine Microstructure, Shanghai Institute of Ceramics, Chinese Academy of Sciences, Shanghai 200050, P. R. China

Supporting Information

ABSTRACT: Photocatalytic water splitting is the most promising process to convert solar energy into high purity chemical fuel (hydrogen), which has received significant attention in recent years. Only several photocatalysts have been reported in the literature for pure water splitting under visible light. Herein we report for the first time quantum sized $BiVO_4$ can decompose pure water into H_2 and O_2 simultaneously under simulated solar light irradiation without any cocatalysts or sacrificial reagents. By electrochemical measurement, we demonstrate that the significantly different photocatalytic activity of the quantum sized $BiVO_4$ arises from the negative shift of conduction band edge by a quantum confinement effect and a decreased overpotential for water reduction. Although the generated H_2 and O_2 are nonstoichiometric in the present study, these findings establish the great potential of using quantum sized $BiVO_4$ photocatalyst and solar energy for overall water splitting.

KEYWORDS: *water splitting, $BiVO_4$ catalyst, solar light, quantum confinement, hydrogen generation*

1. INTRODUCTION

Solar hydrogen generation from semiconductor photocatalysts is considered to be one of the most promising solutions to the global energy crisis.[1−3] Compared with the traditional sulfide photocatalyst, oxide semiconductors are more stable for photocatalytic water splitting and have been widely studied up to the present. A variety of oxide semiconductors, such as $In_{1-x}Ni_xTaO_4$,[2] GaN-ZnO,[4] and $Pt/ZrO_2/TaON$-Pt/WO_3 Z-scheme systems,[5] have been reported for overall water splitting into H_2 and O_2 under visible light. However, these complex oxides required complicated processes to prepare, and a cocatalyst is generally needed. Developing a cost-effective and active solar light driven water splitting photocatalyst is still a great challenge.

The major kinetics limitation for water splitting is the water oxidation reaction, which involved a multielectron transfer process.[6] Among the recently developed oxide semiconductors, bismuth vanadate ($BiVO_4$) has obtained sustaining attention because of its high activity for O_2 evolution under visible light.[7−9] However, $BiVO_4$ as a single photocatalyst for H_2 evolution under visible light has not yet been reported, because the conduction band bottom of $BiVO_4$ is located very close to the H_2 evolution potential (0 V vs NHE at pH 0),[10−12] making the deficient power of photogenerated electrons for H^+ reduction. Consequently, overall water splitting on a single $BiVO_4$ photocatalyst under visible-light irradiation is expected to be achieved if the conduction band bottom could be elevated.

Previous studies have proved that semiconductor nanocrystals exhibit size-dependent optical and photophysical properties that arise from the characteristic electronic structure of nanosized semiconductors.[13−15] When the size of a semiconductor is below its Bohr radius, the magnitude of the band gap energy is critically dependent on the particle size because of a quantum confinement effect. CdSe nanoribbons,[16] CoO nanocrystals,[17] and Co_3O_4 quantum dots[18] have been found showing a high quantum yield for photocatalytic H_2 evolution under visible-light irradiation. These recent studies inspired us to investigate the feasibility of photocatalytic H_2 evolution on quantum sized $BiVO_4$ if its conduction band edge could be elevated by a quantum confinement effect. Herein, we provide the first experimental confirmation of H_2 evolution on quantum sized $BiVO_4$. The quantum confinement effect on the optical, optoelectronic, and electrochemical properties that significantly influence the photocatalytic performance were discussed detailed in this manuscript.

2. EXPERIMENTAL SECTION

2.1. Chemicals and Reagents. All the reagents were of analytical purity and were used as received from Shanghai Chemical Company without further purification.

2.2. Preparation. Quantum sized $BiVO_4$ was prepared according to the previously reported hydrothermal method.[19] Typically, sodium oleate (1.3 mmol) and $Bi(NO_3)_3{\cdot}5H_2O$ (0.4 mmol) were successively added to distilled water (20 mL). An aqueous solution (20 mL) containing $Na_3VO_4{\cdot}12H_2O$ (0.4 mmol) was then injected into the above solution. After vigorous stirring for 2 h, the mixture was transferred to a 50 mL

Received: July 25, 2014
Revised: August 25, 2014
Published: August 27, 2014

   dx.doi.org/10.1021/cs501076a | ACS Catal. 2014, 4, 3498−3503

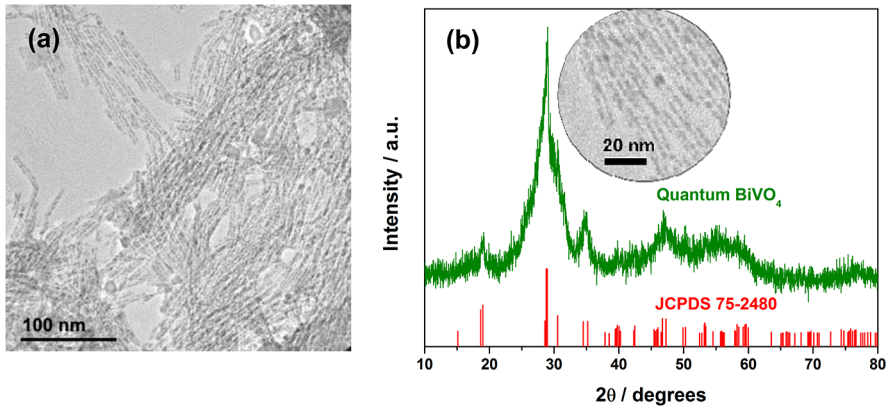

Figure 1. TEM image (a) and XRD pattern (b) of the synthetic quantum sized $BiVO_4$. Inset of b: Higher magnification TEM image of the quantum sized $BiVO_4$.

Teflon-lined autoclave, sealed, and heated at 100 °C for 12 h. The system was then allowed to cool down to room temperature. The obtained solid products were collected by centrifugation, washed with *n*-hexane and absolute ethanol many times, and then freeze-dried for further characterization. For comparison, nanoscale $BiVO_4$ was prepared by solvothermal synthesis method in glycol without the addition of sodium oleate.

2.3. Characterization. The purity and the crystallinity of the as-prepared samples were characterized by powder X-ray diffraction (XRD) on a Japan Rigaku Rotaflex diffractometer using Cu Kα radiation, while the voltage and electric current were held at 40 kV and 100 mA. The transmission electron microscope (TEM) analyses were performed by a JEOL JEM-2100F field emission electron microscope. X-ray photoelectron spectroscopy (XPS) were obtained by irradiating every sample with a 320 μm diameter spot of monochromated aluminum Kα X-rays at 1486.6 eV under ultrahigh vacuum conditions (performed on ESCALAB 250, THERMO SCIENTIFIC Ltd.). UV−vis diffuse reflectance spectra (DRS) of the samples were measured using a Hitachi UV-3010PC UV−vis spectrophotometer. The photoluminescence (PL) spectra were measured with a Hitachi F4600 fluorescence spectrophotometer (excitation wavelength = 340 nm) at room temperature in air.

2.4. Electrochemical Measurements. Electrochemical measurements were performed on a CHI 660D electrochemical workstation (Shanghai Chenhua, China) using a standard three-electrode cell with a working electrode, a platinum wire as counter electrode, and a standard saturated calomel electrode (SCE) in saturated KCl as reference electrode. The working electrodes were prepared by dip-coating: Briefly, 10 mg of photocatalyst was suspended in 0.15 mL of ethanol in the presence of 1% Nafion to produce slurry, which was then dip-coated onto a 2 cm × 1.5 cm FTO glass electrode and drying at 25 °C.

2.5. Photocatalytic Test. Photocatalytic H_2 evolution was conducted in a gas-closed circulation system of a Pyrex cell with a top quartz window. The photocatalyst powder (15 mg) was dispersed by a magnetic stirrer in deionized water (200 mL) or an aqueous solution (200 mL) containing 30 mL of methanol. This suspension was irradiated by a 500 W Xe lamp. The temperature of the suspension system was maintained at room temperature (25 °C) by providing a flow of cooling water during the photocatalytic reaction. The amount of H_2 evolved was determined with online gas chromatography equipped with a thermal conductivity detector (TCD). Nitrogen was purged through the cell before reaction to remove residual air.

3. RESULTS AND DISCUSSION

Figure 1a shows the TEM image of the quantum sized $BiVO_4$, which exhibit a tube-like morphology with an average diameter of 5 nm and nanoscale lengths. A close TEM image indicates (inset of Figure 1b) the tube-like morphology is constructed by interconnected quantum dots with diameter of about 2 nm. The quantum size of the as-prepared sample was also revealed by its XRD pattern which exhibits an obvious widened diffraction peaks of monoclinic $BiVO_4$ (JCPDS No. 75-2480) (Figure 1b). No other impurities were detected from its XRD pattern. For comparison, nanoscale $BiVO_4$ was prepared by a solvothermal synthesis without the assistant of sodium oleate. The average grain size of the nanoscale $BiVO_4$ was about 50 nm both from its XRD pattern and TEM image (Figure S1).

To investigate the photocatalytic water splitting properties of the quantum sized $BiVO_4$, 15 mg of the as-prepared powder sample was dispersed in 200 mL of deionized water in a Pyrex cell with a quartz window on top. After removing residual air through nitrogen purging, the reaction mixture was irradiated under a 500 W xenon arc lamp, while the amount of evolved H_2 was analyzed by online gas chromatography. Figure 2 a shows hydrogen evolution versus time for quantum sized and nanoscale $BiVO_4$ samples. It was found simulated solar light irradiation resulted in continuous H_2 evolution from pure water by quantum sized $BiVO_4$ photocatalyst. The amount of the H_2 generated by the quantum sized $BiVO_4$ was 5.3 μmol after 24 h. When the reaction was performed in 15% aqueous methanol, a known sacrificial electron donor, the hydrogen evolution rate was significantly improved, producing a total H_2 amount of 66.8 μmol after 24 h (Figure 2b), equivalent to a turnover number of 1.44. This suggests that H_2 evolution under these conditions is catalytic. The increase in the H_2 evolution rate in aqueous methanol indicates the quantum sized $BiVO_4$ is able to photo-oxidize methanol. Under the same conditions, no H_2 evolution was detected with the nanoscale $BiVO_4$ photocatalyst both in pure water and aqueous methanol, indicating the poor reduction power of the photogenerated electrons in nanoscale $BiVO_4$ when comparing with that of quantum sized $BiVO_4$ photocatalyst.

To investigate the origin of the H_2 evolution property, the optical property of quantum sized $BiVO_4$ and nanoscale sample

dx.doi.org/10.1021/cs501076a | *ACS Catal.* 2014, 4, 3498−3503

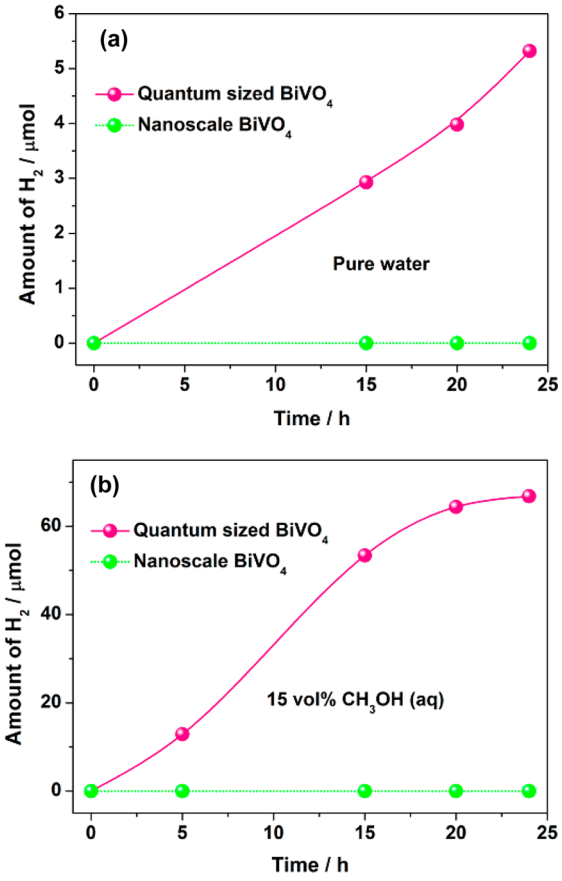

Figure 2. Hydrogen evolution from 15 mg of $BiVO_4$ samples in pure water (a) and 15% methanol aqueous solution (b).

were studied by UV−visible absorption and photoluminescence (PL) spectra. As shown in Figure 3a, The UV−vis diffuse reflectance spectrum of the nanoscale $BiVO_4$ exhibits strong absorption in the visible range with a steep absorption edge shorter than 540 nm. The band gap of the nanoscale $BiVO_4$ was estimated about 2.4 eV according to the Tauc plots in Figure 3b. Different from the steep absorption of nanoscale $BiVO_4$, quantum sized $BiVO_4$ exhibit a nonsteep absorption edge with an obvious absorption shoulder around 430 nm. The nonsteep and dual absorption may be ascribed to its particular morphology which has quantum sized diameter and nanoscale length. From Figure 3a, it was found the upper inflection point of the UV−vis absorption spectrum was blue-shifted from 465 nm for nanoscale $BiVO_4$ to 365 nm for quantum sized $BiVO_4$ sample. Furthermore, the quantum sized $BiVO_4$ exhibited a broad background absorbance in the visible region. This absorption may be attributed to surface defect states[20] or the room-temperature exciton absorption in quantum confined semiconductor.[21] The quantum sized $BiVO_4$ exhibited an increased band gap of 2.72 eV by Tauc plots, although the increase is partially obscured by its intense background absorbance in the visible region. This is an incipient indication of quantum confinement effect in the quantum sized $BiVO_4$ sample. Fluorescence (PL) spectrum also revealed the multiple optical response of the quantum sized $BiVO_4$ sample. The fluorescence emissions which were induced by the surface electronic behaviors are highly dependent on the surface atomic states. As shown in Figure 3c, the nanoscale $BiVO_4$ showed broad photoluminescence spectrum from 470 to 600 nm, which

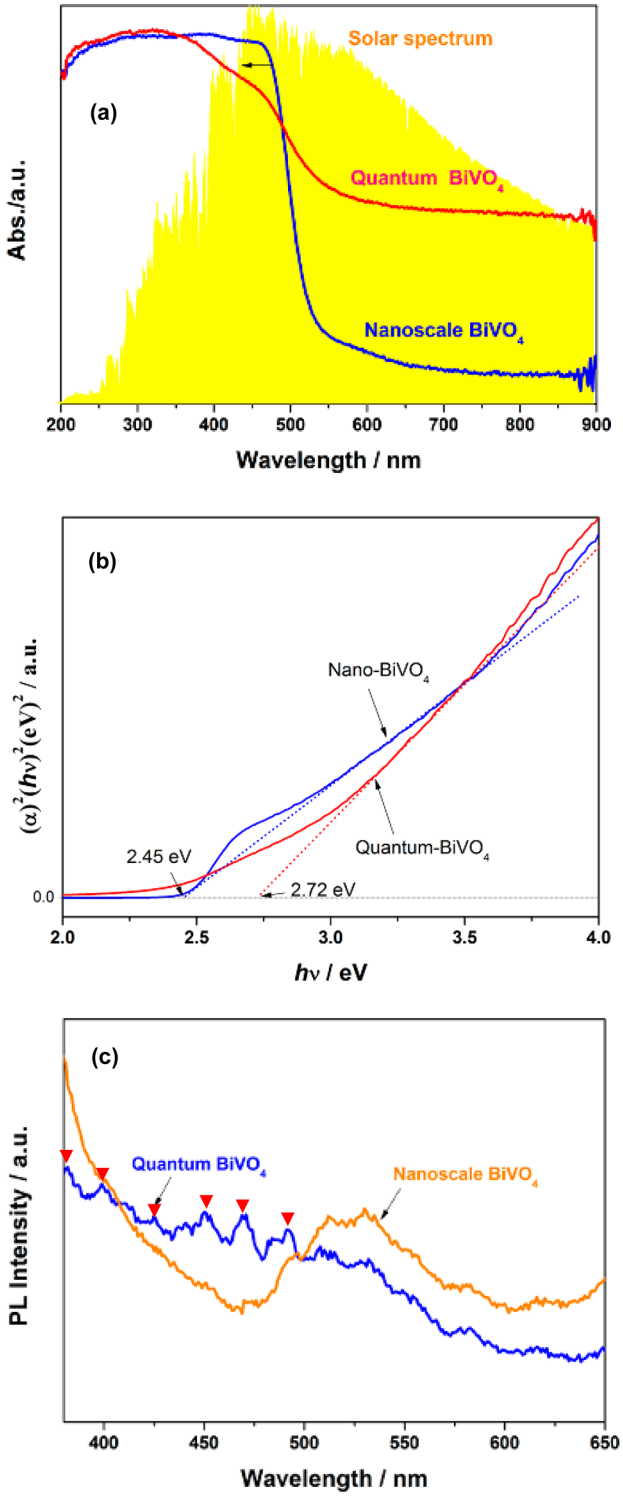

Figure 3. (a) UV−vis diffuse reflection spectra of the quantum sized $BiVO_4$ and nanoparticles. (b) Tauc plots for direct transitions of $BiVO_4$ samples. (c) Photoluminescent spectra of quantum sized $BiVO_4$ and nanoparticles excited at 340 nm at room temperature.

have been reported in the literature.[22,23] The blue edge onset position of the emission spectrum (470 nm) was very close to the upper inflection point of the UV−vis absorption spectrum (465 nm, Figure 3a), indicating that the emission was derived from the band gap excitation. Different from nanoscale $BiVO_4$, the $BiVO_4$ quantum tube exhibited more complex multicolor emissions. Besides the emission peaks around 510 and 530 nm

dx.doi.org/10.1021/cs501076a | ACS Catal. 2014, 4, 3498−3503

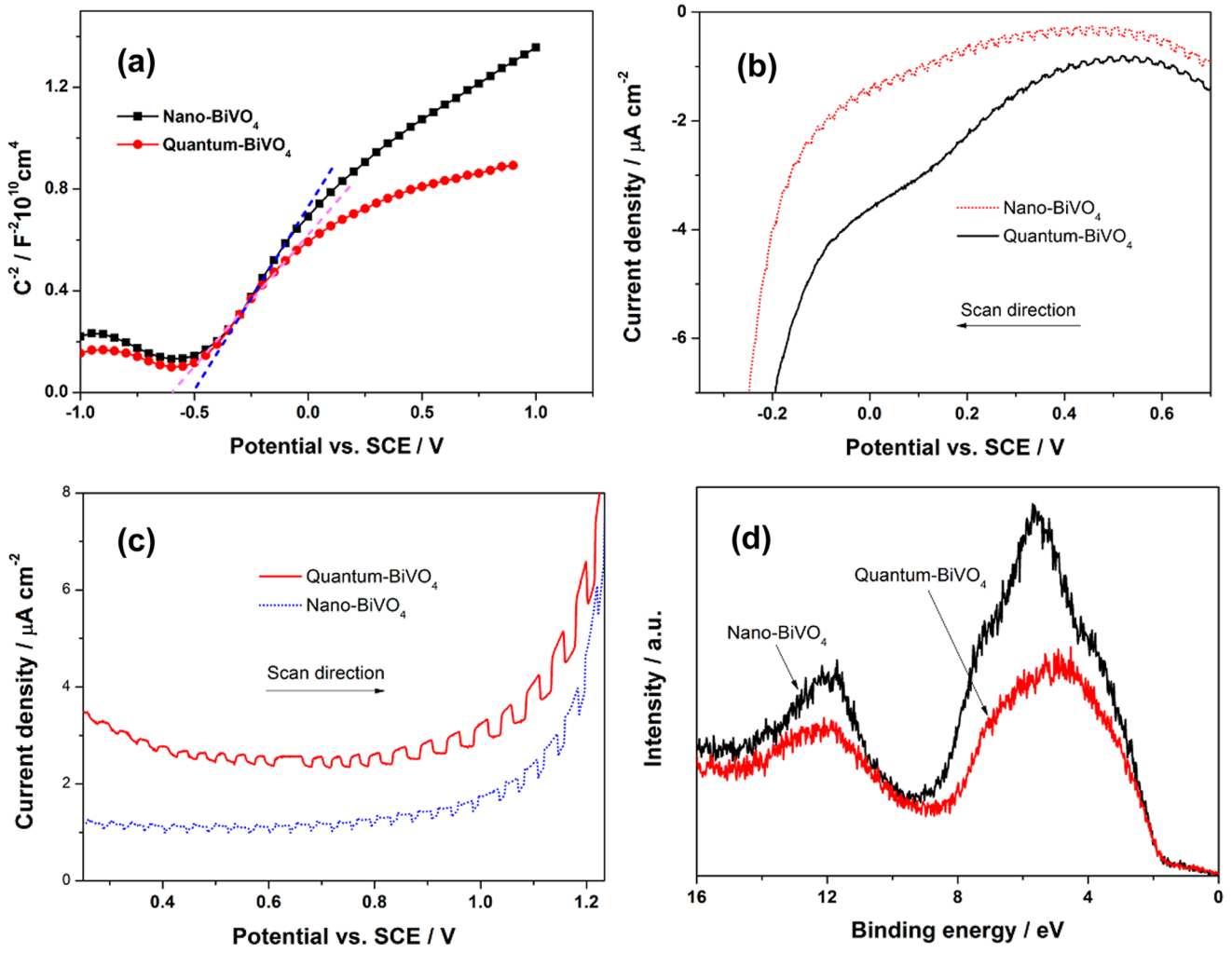

Figure 4. (a) Mott−Schottky plots of the synthetic quantum sized $BiVO_4$ and nanocrystals. (b) Cathodic and (c) anodic electrochemical scans on the synthetic $BiVO_4$ films under chopped simulated solar light irradiation. (d) XPS valence band spectra of the synthetic $BiVO_4$ samples.

which are similar to nanoscale $BiVO_4$, six other obvious emission peaks centered around 382, 399, 425, 450, 469, and 491 nm were also observed (red trigons marked in Figure 3c). These discontinuous emissions may be come from the discrete energy levels in a quantum confined semiconductor which has been observed by Bayer et al. in InGaAs QDs.[24] The emergence of the blue-shifted photoluminescence peaks with wavelength shorter than 470 nm revealed the existence of high energy electron−hole pairs in the photoexcited quantum sized $BiVO_4$ sample and also is a direct evidence of energy band splitting by quantum confinement effect.

Further insight into the differences in photocatalytic activity of the quantum sized and nanoscale $BiVO_4$ samples were obtained using photoelectrochemical measurements. The flat-band potential (E_{fb}) of semiconductor electrode is usually measured by Mott−Schottky analysis.[25] Figure 4a shows the Mott−Schottky plot of the quantum sized and nanoscale $BiVO_4$ electrodes, which was generated from the capacitance values measured at 1000 Hz in the dark. The positive slope of the plot indicates the presence of a characteristic n-type semiconductor and that electrons are the majority charge carriers. The E_{fb} value was calculated from the intercept of the axis with potential values. The E_{fb} of the nanoscale $BiVO_4$ measured in this analysis was −0.26 V vs NHE (−0.5 V vs SCE) at pH 7, while the quantum sized $BiVO_4$ exhibits an obvious negative shift of E_{fb} which located at −0.36 V vs NHE (−0.6 V vs SCE) under the same conditions. E_{fb} is strongly related to the bottom of the conduction band (E_{cb}) and is considered to be about 0.1 V below the E_{cb} for many n-type semiconductors.[26,27] A shift of E_{cb} to more reducing potentials can be taken as the third manifestation of the quantum confinement effect, in addition to the blue-shifted absorption and discrete fluorescence emissions spectra.

Voltammetry scans were performed to directly determine the over potentials for water oxidation and water reduction by the different $BiVO_4$ samples on FTO conducting substrate in 0.5 M Na_2SO_4 solution at pH 7 (Figure 4b,c). As shown in Figure 4b, cathodic scans revealed the overpotential for water reduction was located at about −0.23 V for the nanoscale $BiVO_4$ film under chopped simulated solar light irradiation. Under the same conditions, the quantum sized $BiVO_4$ exhibited much lower reduction overpotential of about −0.1 V, indicating a much easier water reduction reaction on quantum sized $BiVO_4$. Anodic scans demonstrated the water oxidation potential on the quantum sized $BiVO_4$ and the nanoscale sample was almost the same (Figure 4c) under chopped simulated solar light irradiation. The water oxidation potential of semiconductor photocatalyst is closely related to its valence band position. X-ray photoelectron spectroscopy (XPS) is a powerful tool to investigate valence band position on the sample surface. As

dx.doi.org/10.1021/cs501076a | ACS Catal. 2014, 4, 3498−3503

shown in Figure 4d, the valence band edge position of the quantum sized $BiVO_4$ was almost identical with that of the nanoscale sample, which may be the origin of the similar water oxidation potential on different $BiVO_4$ samples. Considering the difference in the band gap is about 0.3 eV between the nanoscale and quantum sized samples from their absorption spectra, the negative shift of E_{cb} for quantum sized $BiVO_4$ may be more than 0.1 eV because the valence band position is almost the same. Here, the deviation of the E_{cb} position may be ascribed to the large number of surface states in quantum sized $BiVO_4$ sample, leading to a change of the band position.[28]

Based on the above analysis, the photocatalytic H_2 evolution property of the quantum sized $BiVO_4$ may arise from its quantum confinement effect on the band structure. Figure 5

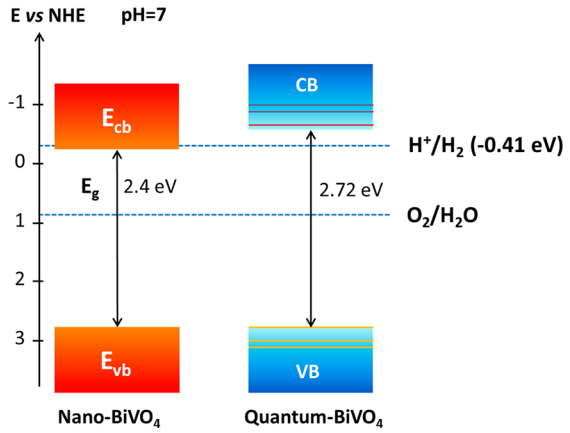

Figure 5. Schematic band structures of nanoscale $BiVO_4$ and quantum sized $BiVO_4$.

shows the approximate band-edge positions of both nanoscale and quantum crystals based on the above-measured flat-band potentials. Here we assumed that conduction band edge was about 0.1 eV above the flat-band potentials for both of the $BiVO_4$ samples. As shown in Figure 5, a qualitative difference exists between nanoscale and quantum crystals in their conduction band edge positions with regard to water reduction potential. Specifically, the conduction band edge position of the nanoscale $BiVO_4$ (−0.36 eV) is located below the hydrogen-evolution potential at pH 7 (−0.41 eV). The photogenerated electrons on nanoscale $BiVO_4$ could not take part in the H^+ reduction half-reaction to evolve H_2 because of their insufficient reduction ability. In contrast, the photogenerated electrons on quantum sized $BiVO_4$ could reduce H^+ to H_2 because the conduction-band edge (−0.46 eV) of quantum sized $BiVO_4$ was shifted above the hydrogen-evolution potential by a quantum confinement effect. Meanwhile, the valence band edge of $BiVO_4$ lies below the oxygen-evolution potential. This band alignment with water redox potentials satisfies the necessary requirement for water splitting, explaining why quantum sized $BiVO_4$ have significantly different photocatalytic activity to that of nanocrystals. However, in the present study it was found the amount of generated O_2 was higher than that of H_2 from pure water splitting on the quantum sized $BiVO_4$ sample (as shown in Figure S2). The reasons for the nonstoichiometric ratio of H_2 and O_2 are not clear at present. Additional studies on the detailed mechanism of water splitting with quantum sized $BiVO_4$ are underway in this laboratory.

4. CONCLUSIONS

We have successfully demonstrated quantum sized $BiVO_4$ exhibits photocatalytic activity for pure water splitting under simulated solar light irradiation. This is the first experimental confirmation of simultaneously water oxidation and reduction by $BiVO_4$ without any cocatalyst. The hydrogen evolution property of quantum sized $BiVO_4$ was mainly ascribed to the negative shift of conduction band edge by a quantum confinement effect. This result emphasized the dependency of E_{cb} on the driving force of photocatalytic water reduction and the possibility of tuning photocatalytic performance through controlling particle size. Considering the excellent photocatalytic water oxidation performance of $BiVO_4$, the present study demonstrated the high potential of quantum sized $BiVO_4$ for overall water splitting using solar light irradiation. These findings are important for optimizing the photocatalytic water splitting performance with semiconductor nanostructures and also for providing new microscopic insights into photocatalytic solar energy conversion.

■ ASSOCIATED CONTENT

Supporting Information

XRD and TEM image of nanoscale $BiVO_4$. Oxygen evolution from quantum sized $BiVO_4$ sample in pure water. This material is available free of charge via the Internet at http://pubs.acs.org.

■ AUTHOR INFORMATION

Corresponding Author

*E-mail: wzwang@mail.sic.ac.cn.

Notes

The authors declare no competing financial interest.

■ ACKNOWLEDGMENTS

This work was financially supported by the National Basic Research Program of China (Grant Nos. 2010CB933503, 2013CB933203), National Natural Science Foundation of China (Grant Nos. 51102262, 51272269), and the Science Foundation for Youth Scholar of State Key Laboratory of High Performance Ceramics and Superfine Microstructures (Grant Nos. SKL201204).

■ REFERENCES

(1) Fujishima, A.; Honda, K. *Nature* **1972**, *238*, 37−38.
(2) Zou, Z.; Ye, J.; Sayama, K.; Arakawa, H. *Nature* **2001**, *414*, 625−627.
(3) Chen, X. B.; Shen, S. H.; Guo, L. J.; Mao, S. S. *Chem. Rev.* **2010**, *110*, 6503−6570.
(4) Maeda, K.; Teramura, K.; Lu, D. L.; Takata, T.; Saito, N.; Inoue, Y.; Domen, K. *Nature* **2006**, *440*, 295−295.
(5) Maeda, K.; Higashi, M.; Lu, D. L.; Abe, R.; Domen, K. *J. Am. Chem. Soc.* **2010**, *132*, 5858−5868.
(6) Zhong, D. K.; Choi, S.; Gamelin, D. R. *J. Am. Chem. Soc.* **2011**, *133*, 18370−18377.
(7) Kudo, A.; Omori, K.; Kato, H. *J. Am. Chem. Soc.* **1999**, *121*, 11459−11467.
(8) Seabold, J. A.; Choi, K. S. *J. Am. Chem. Soc.* **2012**, *134*, 2186−2192.
(9) Wang, D.; Li, R.; Zhu, J.; Shi, J.; Han, J.; Zong, X.; Li, C. *J. Phys. Chem. C* **2012**, *116*, 5082−5089.
(10) Sayama, K.; Nomura, A.; Arai, T.; Sugita, T.; Abe, R.; Yanagida, M.; Oi, T.; Iwasaki, Y.; Abe, Y.; Sugihara, H. *J. Phys. Chem. B* **2006**, *110*, 11352−11360.

(11) Kohtani, S.; Yoshida, K.; Maekawa, T.; Iwase, A.; Kudo, A.; Miyabe, H.; Nakagaki, R. *Phys. Chem. Chem. Phys.* **2008**, *10*, 2986−2992.
(12) McDonald, K. J.; Choi, K. S. *Energy Environ. Sci.* **2012**, *5*, 8553−8557.
(13) Rossetti, R.; Ellison, J. L.; Gibson, J. M.; Brus, L. E. *J. Chem. Phys.* **1984**, *80*, 4464−4469.
(14) Brus, L. E. J. *Chem. Phys.* **1984**, *80*, 4403−4409.
(15) Nascimento, C. C.; Andrade, G. R. S.; Neves, E. C.; Barbosa, C. D. E. S.; Costa, L. P.; Barreto, L. S.; Gimenez, I. F. *J. Phys. Chem. C* **2012**, *116*, 21992−22000.
(16) Frame, F. A.; Carroll, E. C.; Larsen, D. S.; Sarahan, M.; Browning, N. D.; Osterloh, F. E. *Chem. Commun.* **2008**, 2206−2208.
(17) Liao, L.; Zhang, Q.; Su, Z.; Zhao, Z.; Wang, Y.; Li, Y.; Lu, X.; Wei, D.; Feng, G.; Yu, Q.; Cai, X.; Zhao, J.; Ren, Z.; Fang, H.; Robles-Hernandez, F.; Baldelli, S.; Bao, J. *Nat. Nanotechnol.* **2014**, *9*, 69−73.
(18) Zhang, N.; Shi, J.; Mao, S. S.; Guo, L. *Chem. Commun.* **2014**, *50*, 2002−2004.
(19) Sun, Y.; Xie, Y.; Wu, C.; Zhang, S.; Jiang, S. *Nano Res.* **2010**, *3*, 620−631.
(20) Townsend, T. K.; Browning, N. D.; Osterloh, F. E. *ACS Nano* **2012**, *6*, 7420−7426.
(21) Miller, D. A. B.; Chemla, D. S.; Eilenberger, D. J.; Smith, P. W.; Gossard, A. C.; Tsang, W. T. *Appl. Phys. Lett.* **1982**, *41*, 679−681.
(22) Chen, L.; Zhang, Q.; Huang, R.; Yin, S. F.; Luo, S. L.; Au, C. T. *Dalton Trans.* **2012**, *41*, 9513−9518.
(23) Zhao, W.; Wang, Y.; Yang, Y.; Tang, J.; Yang, Y. *Appl. Catal., B* **2012**, *115*−*116*, 90−99.
(24) Bayer, M.; Stern, O.; Hawrylak, P.; Fafard, S.; Forchel, A. *Nature* **2000**, *405*, 923−926.
(25) Watanabe, A.; Kozuka, H. *J. Phys. Chem. B* **2003**, *107*, 12713−12720.
(26) Matsumoto, Y. *J. Solid State Chem.* **1996**, *126*, 227−234.
(27) Ishikawa, A.; Takata, T.; Kondo, J. N.; Hara, M.; Kobayashi, H.; Domen, K. *J. Am. Chem. Soc.* **2002**, *124*, 13547−13553.
(28) Hagfeldt, A.; Bjorksten, U.; Gratzel, M. *J. Phys. Chem.* **1996**, *100*, 8045−8048.